Dalton Transactions

PAPER

View Article Online
View Journal | View Issue

Cite this: *Dalton Trans.*, 2015, **44**, 11551

A family of Ru(II) complexes built on a novel sexipyridine building block: synthesis, photophysical properties and the rare structural characterization of a triruthenium species†

Baptiste Laramée-Milette,[a] Félix Lussier,[a] Ilaria Ciofini*[b] and Garry S. Hanan*[a]

Received 11th February 2015,
Accepted 15th May 2015

DOI: 10.1039/c5dt00631g

www.rsc.org/dalton

A new tris-2″,4″,6″-(2,2′-bipyridin-4-yl)-1″,3″,5″-triazine ligand and its family of ruthenium coordination complexes are described along with their characterization by electrochemical and photophysical methods as well as a rare single crystal X-ray analysis of a triruthenium polypyridine complex.

Introduction

Over the past few years, the 1,3,5-triazine motif has become an important molecular component in the field of organic, supramolecular and coordination chemistry due to its diverse reactivity as well as its electronic and structural properties.[1] As a consequence, triazine-containing compounds have found applications in multiple domains, such as catalysis,[2] medicinal chemistry,[3] polymer chemistry[4] as well as a considerable contribution to the herbicide industry.[5] In addition, several examples of well-designed triazine ligands were used as building blocks for applications in inorganic self-assembly, a highly active field in modern supramolecular chemistry, in which the coordination of transition metal ions with appropriate ligands can lead to higher nuclearity species.[6]

Ruthenium complexes of triazine-based ligands are of interest due to their desirable photophysical (*e.g.*, predictable absorption and emission energies) and electrochemical (*e.g.*, multi-electron storage) properties, which are easily tuned by modifying the ligand surrounding the metal core.[7] Such complexes have already found uses in a wide variety of photosensitization applications, as switches,[8] molecular engines,[9] dye-sensitized solar cells[10] and light-harvesting antennae,[11] however, the intensity of light absorption in the visible portion of the spectrum is often relatively low as compared to intense absorption based on some organic dyes such as dipyrromethenes[12] and porphyrins.[13]

Herein, we report the synthesis and the properties of a new family of ruthenium complexes $[(Ru(2,2'\text{-bpy})_2)_n(L)][(PF_6)_{2n}]$, where n = 1, 2 and 3 (abbreviated as **RuL**, **Ru$_2$L** and **Ru$_3$L** in the text; see Chart 1) with a 1,3,5-triazine bridging ligand **L**. The ligand was designed to enhance the electronic delocalization of the acceptor orbital of the metal-to-ligand charge-transfer (MLCT) transitions. The concomitant red-shift in the absorption energy and the increase in the molar absorptivity as a whole greatly enhances overall light absorption.

Results and discussion

Tris-4-(2,2′-bipyridine)-1,3,5-triazine ligand: synthesis, NMR spectroscopy and solid state characterization

The starting 4-cyano-2,2′-bipyridine precursor was prepared according to a previously published Negishi-type heterocoupling reaction and was obtained in good yield (85%).[14] Following a similar methodology employed by Case,[15] the starting material was then melted at 180 °C in the presence of a catalytic amount of NaH in anhydrous conditions under an inert atmosphere (Scheme 1). The resulting brown slurry was heated for eight hours and the reaction was then quenched with ethanol and water. The pure tris-2″,4″,6″-(2,2″-bipyridin-4-yl)-1″,3″,5″-triazine (**L**) was recovered in moderate yield (60%) as a pure beige precipitate by simple filtration, without the need of any further purification (Scheme 1 and Fig. 1).

Single crystals suitable for X-ray diffraction were obtained by slow evaporation of a dichloromethane solution of **L**. As shown in Fig. 2, the introduction of nitrogen atoms into the core heterocyclic ring permit the 2,2′-bipyridine and triazine portions of **L** to lie co-planar which in turn enhances electron-delocalization throughout the system.

[a]*Département de Chimie, Université de Montréal, Montréal, Québec, Canada, H3 T 2B1. E-mail: garry.hanan@umontreal.ca*
[b]*PSL Research University, Institut de Recherche de Chimie Paris IRCP, CNRS – Chimie ParisTech, 11 rue Pierre et Marie Curie, F-75005 Paris, France*

†Electronic supplementary information (ESI) available: Experimental section and crystallographic data, additional figures, nuclear resonance magnetic analysis, high-resolution mass spectrometry, cyclic voltammogram and DFT calculation. CCDC 964307 and 1017168. For ESI and crystallographic data in CIF or other electronic format see DOI: 10.1039/c5dt00631g

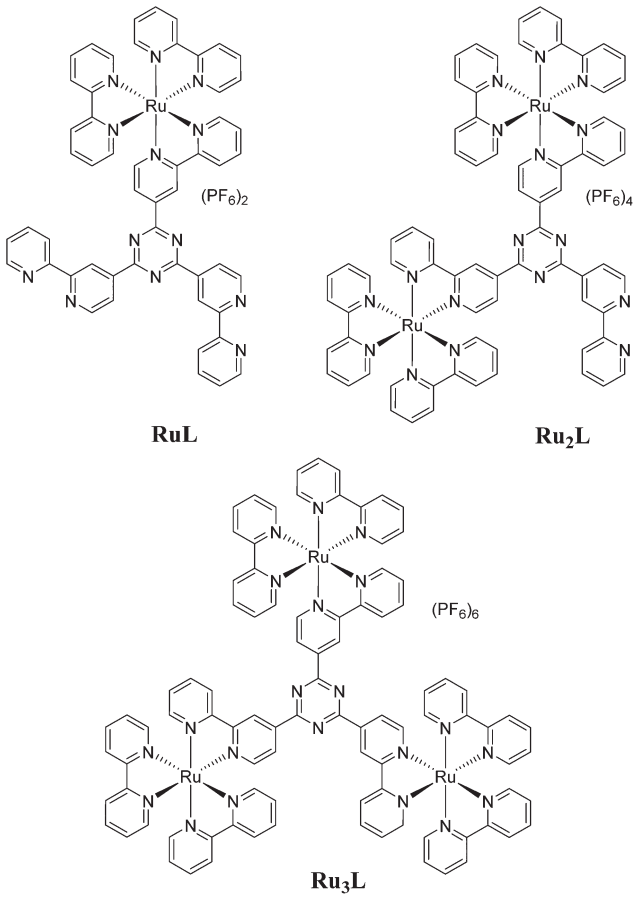

Chart 1 Molecular structures of **RuL**, **Ru_2L** and **Ru_3L**.

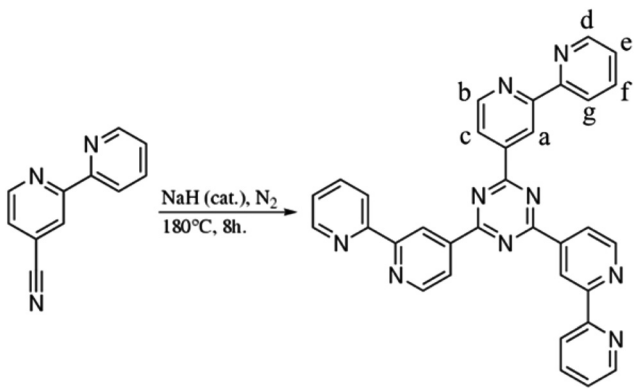

Scheme 1 Synthesis of ligand tris-2″,4″,6″-(2,2″-bipyridin-4-yl)-1″,3″,5″-triazine (**L**).

Two of the 2,2′-bipyridine subunits are almost perfectly co-planar with the triazine ring, with torsion angles of less than 5°. The torsion angle of the third bpy subunit is of 24.1°, which is significantly different from the two other "arms" of the molecule. As shown in Fig. 3, π-stacking appears to be at the origin of the observed deviation from planarity, where the centroid–centroid separation (R_{cent}) and the distance between

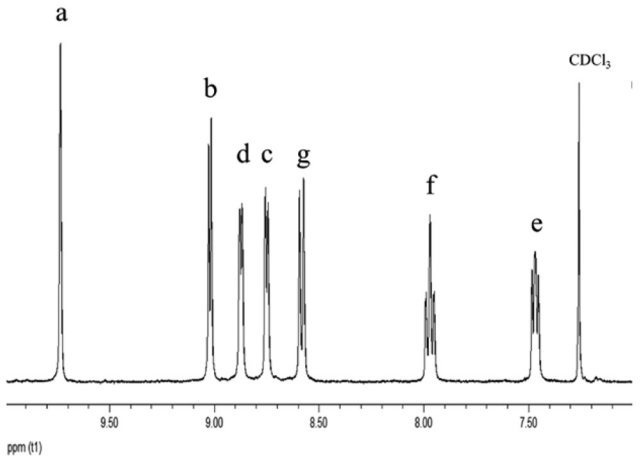

Fig. 1 Aromatic region of the 400 MHz ^{1}H NMR spectrum of ligand **L** in $CDCl_3$. See Scheme 1 for the atom labelling.

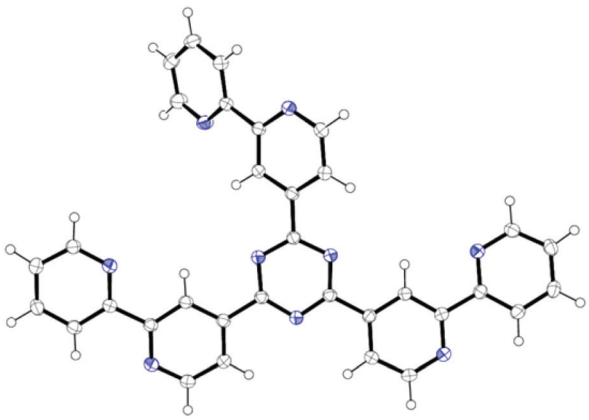

Fig. 2 X-ray crystal structure of ligand **L**. The ellipsoids are drawn with a 50% probability.

the closest atoms ($R_{closest}$) are found to be 4.09 Å and 3.65 Å, respectively, with an interplanar angle (θ_{plane}) of 18.5°.

Ru(II) polypydines metal complexes: synthesis, ^{1}H NMR and solid state characterization

The mono- and diruthenium metal complexes were prepared by conventional thermal synthesis, by refluxing a 1 : 2 ratio of ligand to metal precursor Ru(2,2′-bipyridyl)$_2$Cl$_2$ in a DCM : MeOH (1 : 2) solution with a slight excess (2.2 eq.) of silver nitrate (used as a dechlorinating agent) over 24 hours. After evaporation of the solvent, the isolated crude product was purified by column chromatography (silica, MeCN : H_2O : KNO_3 sat. 7 : 2 : 1) where **RuL** and **Ru_2L** were recovered in a 29% and 21% yield, respectively.

The triruthenium metal complex was prepared by both thermal and microwave syntheses, by using a 3-fold excess of the ruthenium precursor, Ru(bpy)$_2$Cl$_2$. In both cases, the yields were similar (60%), the advantage of microwave

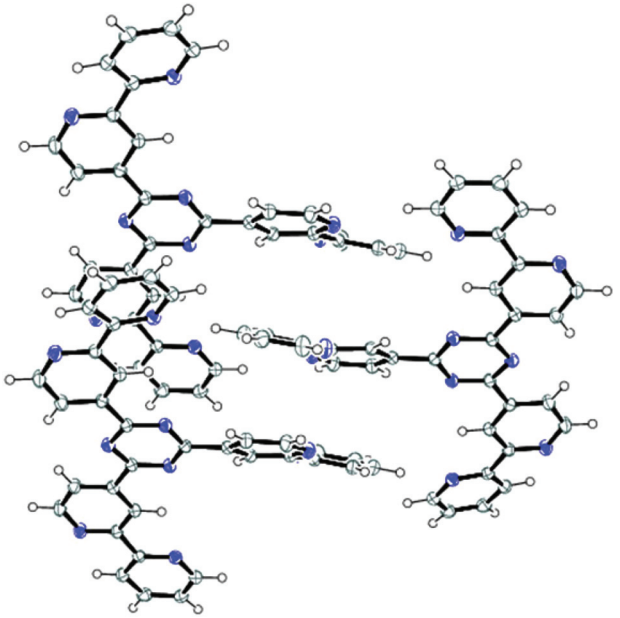

Fig. 3 Packing of ligand L with distances as short as 3.65 Å between π-stacked bipyridine arms.

irradiation being the shorter reaction time of 10 minutes instead of 4 hours. In both cases, a solvent mixture of ethylene glycol : water (9 : 1) was kept under reflux in the presence of $AgNO_3$ as the dechlorinating agent. The isolated crude product was purified by column chromatography, using the exact same conditions for the elution. It is worth mentioning that in both thermal and microwave syntheses, no traces of the mono- and bimetallic species were found.

Singles crystals suitable for X-ray diffraction were obtained by slow diffusion of diisopropyl ether into an acetonitrile solution of **[Ru$_3$L][(BF$_4$)$_6$]** over several weeks (Table 1). The asymmetric unit display the main molecule with the counter-anions and three solvent molecules (see Fig. S12†). Singles crystals were also obtained by the same procedure with **[Ru$_3$L][(PF$_6$)$_6$]**, however, the rapid decomposition of the crystals once removed from the mother liquor motivated our choice to try other counter-anions. The ruthenium stereocenter can adopt either the Λ or Δ configuration, which gives rise to a mixture of stereoisomers. Due to the presence of an inversion center in the space group ($P2_1/c$) as well as disorder around one of the metal cores (see Fig. S13†), the species is not enantiopure: the four isomers (Λ,Λ,Λ; Δ,Δ,Δ; Δ,Δ,Λ and Λ,Λ,Δ) can be observed by X-ray diffraction. For the sake of clarity, only two of the four isomers are displayed in Fig. 4.

The Ru–N bond lengths range between 2.01–2.08 Å, which is comparable to the distance found in the parent $[Ru(2,2'\text{-bpy})_3]^{2+}$ complex (2.04–2.06 Å).[16] The distance between the metal centers range between 12.8–13.6 Å. The angle found between the core of the triazine and each of the 2,2′-bipyridyl arms lie between 15° and 27° (Ru1 unit = 26.6°; Ru2 unit = 15.5°; Ru3 unit = 21.6°) which differ significantly when compare to the values observed in the free ligand. As depicted in Fig. 5 and 6, the bulky nature of the trinuclear complex most likely induces this deviation from planarity due to packing.

Table 1 Solid-state structure and refinement data for ligand L and complex **Ru$_3$L**

	L	Ru$_3$L
Formula	$C_{33}H_{21}N_9$	$[C_{93}H_{69}N_{21}Ru_3][(BF_4)_6]\cdot(CH_3CN)_3$
M_w [g mol^{-1}]	543.59	2427.30
Temperature [K]	173(2)	100(2)
Wavelength [Å]	1.54178	1.34139
Crystal system	Monoclinic	Monoclinic
a [Å]	8.33110(10)	22.8909(7)
b [Å]	19.4283(2)	13.6566(4)
c [Å]	16.2362(2)	35.3984(12)
α [°]	90	90
β [°]	103.8550(10)	91.874(2)
γ [°]	90	90
V [Å^3]	2551.52(5)	11060.0(6)
Space group	$P2_1/n$	$P2_1/c$
Z	4	4
$d_{calcd.}$ [g cm^{-3}]	1.415	1.458
μ [m ml^{-1}]	0.711	2.760
F(000)	1128	4871
Reflection collected	50 021	230 761
Independent reflections	4850	22 119
GoF	1.019	1.037
$R_1(F)$ [$I > 2\sigma(I)$]	0.0347	0.0731
w$R(F^2)$ [$I > 2\sigma(I)$]	0.0932	0.2023
$R_1(F)$ (all data)	0.0405	0.1023
w$R(F^2)$ (all data)	0.0982	0.2174
Largest difference peak/hole [e Å^{-3}]	0.204/−0.211	1.542/−1.147

Analysis of the ^{1}H NMR of the Ru(II) complexes indicates that the correct number of proton resonances are found in the aromatic region of the spectrum (Fig. 7), however, detailed assignments were not established.

The singlets found above 9.5 ppm can be assigned to the proton located near the triazine core (labeled as "a" in Scheme 1). As displayed in Fig. 7, only one singlet is found near 9.6 ppm in the case of **Ru$_3$L**, since the three protons are equivalent due to a C_3 rotation axis. Two singlets, corresponding to the coordinated and non-coordinated 2,2′-bipyridyl arms, are found in the case of the **Ru$_2$L** compounds. It is worth mentioning that similar behaviour was observed in the case of the **RuL** species. It appears that the ^{1}H NMR spectrum for that specific compound is concentration dependent, which precludes complete comparison with the **Ru$_2$L** and **Ru$_3$L** species. Such behavior had already been reported and might be a consequence of molecular aggregation.[17]

Photophysical properties

The 1,3,5-triazine ligand exhibits up to four absorption bands with $\lambda_{max} \approx 246$, 253, 279 and 322 nm (see ESI, Fig. S10†), which are attributed to the $\pi \rightarrow \pi^*$ transition centered on the 2,2′-bipyridyl and the 1,3,5-triazine units (Table 2). The free ligand is a blue emitter in solution, with an emission maximum centered at 412 nm (see Fig. S11†). It is worth mentioning the exceptional broad emission profile of about

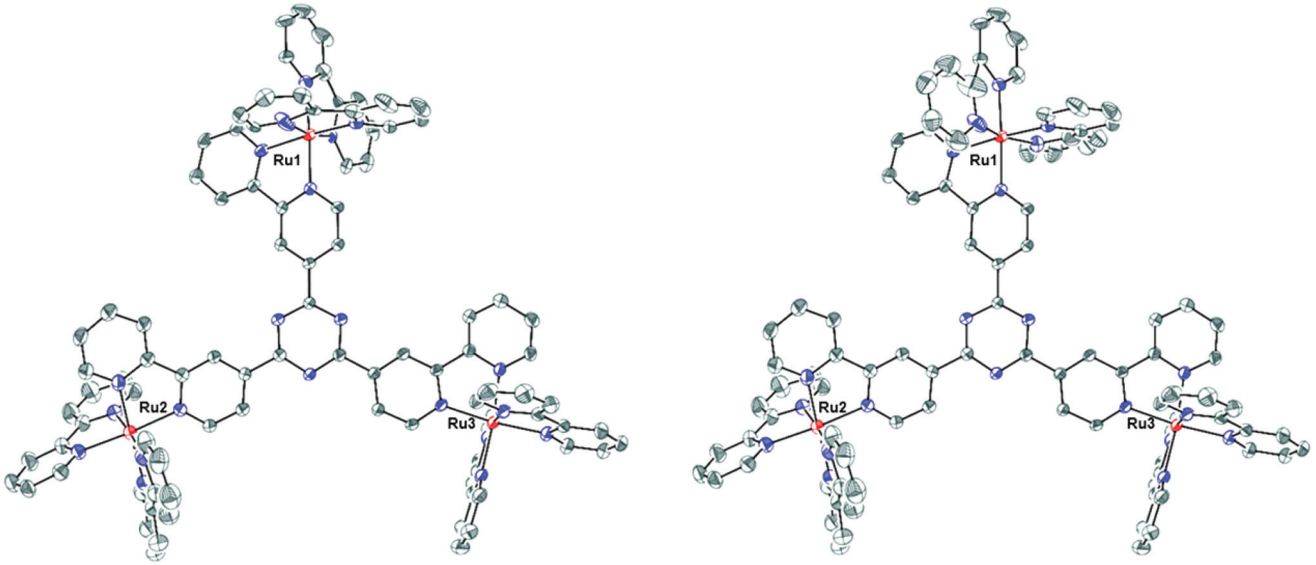

Fig. 4 X-Ray crystal structure of Ru_3L from top view exposing the Δ,Δ,Δ (left) and Λ,Δ,Δ (right) enantiomers with ellipsoids plotted at a 30% probability level. The solvent molecules (acetonitrile), the hydrogen atoms as well as the BF_4 counter-anions have been omitted for clarity.

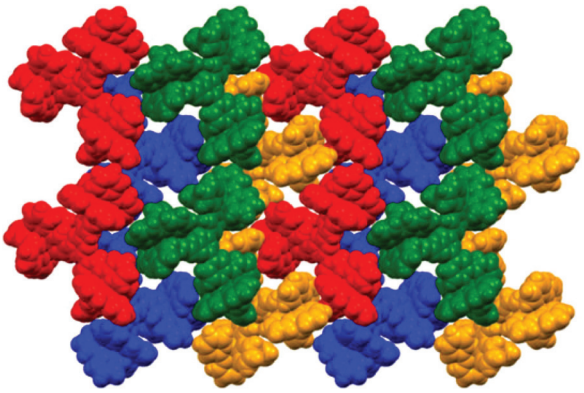

Fig. 5 Spacefilling view down the *b* axis showing the crystal packing.

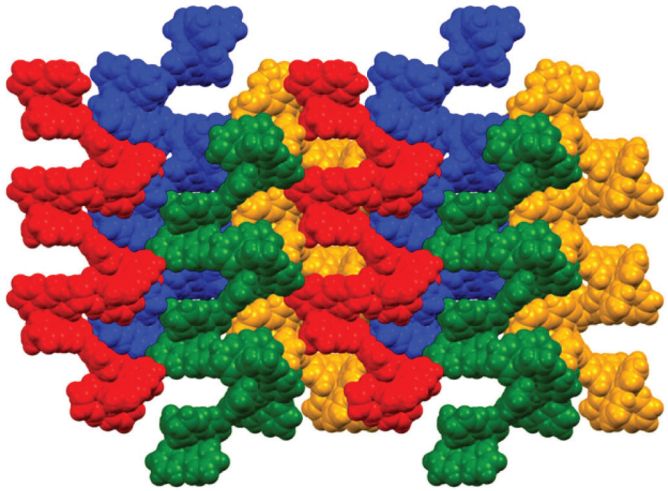

Fig. 6 Crystal packing viewed down the *a* axis which shows the herring-bone type packing.

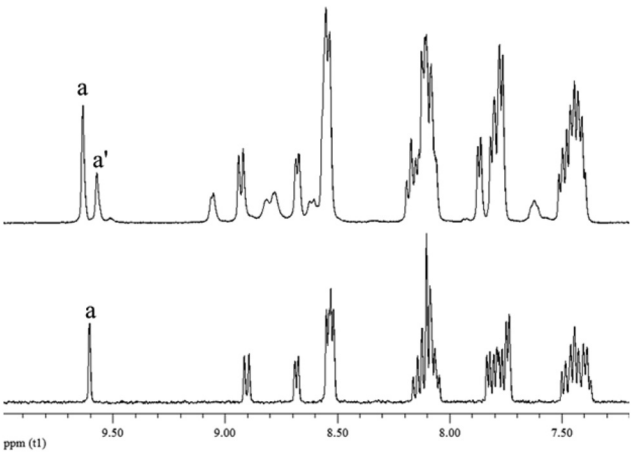

Fig. 7 ^{1}H NMR of **Ru_2L** (top) and **Ru_3L** (bottom) in the 7–10 ppm region.

400 nm (325–725 nm) as compared to the typical 2,2′-bipyridyl ligand, which display roughly half the emission profile of ligand **L** (300–500 nm).[18]

The absorption spectra of the three metal complexes and the reference $[Ru(2,2'\text{-bpy})_3][(PF_6)_2]$ are shown in Fig. 8 and their data are collected in Table 2. All of the Ru(II) complexes exhibit intense ligand-centered (LC) bands in the UV region (200–350 nm). These bands can be attributed to π–π* transitions in the aromatic bpy and triazine part of the molecule. The shoulder peak at ~325 nm, which is missing in the reference, can be attributed to intra-ligand electronic transitions involving the 1,3,5-triazine core. Also, MLCT bands are present in the visible portion (380–700 nm) of the spectrum and they display enhanced absorptivity coefficients as compared to the $[Ru(2,2'\text{-bpy})_3]^{2+}$ species. A red-shift of the MLCT band of Ru-

Table 2 Absorption maxima for the ligand, metal complexes and the references

Compound	Absorption λ_{max}/nm (ε, $\times 10^4$ M^{-1} cm^{-1})
2,2′-bpy[a]	238 (1.14), 244 (1.03), 283 (1.47)
L[a]	246 (6.28), 253 (6.29), 279 (3.58), 322 (1.08)
RuL^{2+} [b]	244 (6.92), 281 (5.91), 444 (1.06), 479(1.23)
Ru_2L $^{4+}$ [b]	246 (8.01), 284 (9.63), 446 (1.97), 487 (2.39)
Ru_3L $^{6+}$ [b]	246 (8.52), 285 (14.3), 442 (2.80), 497 (3.79)
$[Ru(bpy)_3]^{2+}$ [b]	244 (2.43), 254 (1.97), 287 (7.18), 423 (0.93), 452 (1.16)

[a] In deaerated dichloromethane. [b] In deaerated acetonitrile.

to-L (497 nm) transition is observed as compared to the reference $[Ru(2,2'\text{-bpy})_3]^{2+}$ complex (452 nm). The greater pi-acceptor ability of the 2,2′-bipyridines attached to the triazine lead to the lower energy transitions. Interestingly, the Ru-to-bpy MLCT transition is blue shifted (442 nm), albeit slightly, as compared to the same transition in $[Ru(2,2'\text{-bpy})_3]^{2+}$. A weaker broad absorption band tails out past 600 nm, which is mostly likely due to spin–orbit coupling.[19]

These results are consistent with the calculated electronic transitions by TD-DFT using the PBE0 functional with inclusion of solvent (acetonitrile) by the conductor-like polarization continuum model (CPCM). The simulated UV/visible electronic absorption spectra of the three Ru(II) complexes are displayed in Fig. 9. Spectra were simulated by convolution of computed vertical excitation using a Gaussian broadening. The area of the bands is proportional to the calculated oscillator strength.

Luminescence spectra of the metal complexes were obtained in acetonitrile solutions (Table 3). The emission spectra are displayed in Fig. 10 and their data are collected in Table 3. Concomitant with the red-shift of the ^{1}MLCT band absorption bands in the visible spectrum as compared to $[Ru(2,2'\text{-bpy})_3]^{2+}$, the ^{3}MLCT emission band is red-shifted from 608 nm to 712 nm. The excited-state lifetime of the ruthenium complexes is shorter compared to the $Ru(2,2'\text{-bpy})_3(PF_6)_2$ reference, as a result of the lower energy excited state which results in faster non-radiative decay as predicted by the Energy Gap Law.[21] Since the energy level of the π^* orbital centered on the triazine ligand is much lower in energy than that centered on the pyridine substituent, the resulting mixed orbital would have dominant contributions from the 1,3,5-triazine orbital (see redox data, figures and DFT calculations in ESI†). The effect of such an energy mismatch was already observed in heteroleptic ruthenium complexes with substituted 4,4′-bipyrimidines[22d] and with Ru(II) complexes containing 2-aryl-4,6-di(2-pyridyl)-*s*-triazine ligands.[22a–c]

Electrochemical properties

The electrochemical properties of the ligand and the Ru(II) complexes have been investigated. The data are summarized in Table 4, and representative cyclic voltammograms are shown in Fig. 11 and S15–S18 (see ESI†). The ligand exhibits

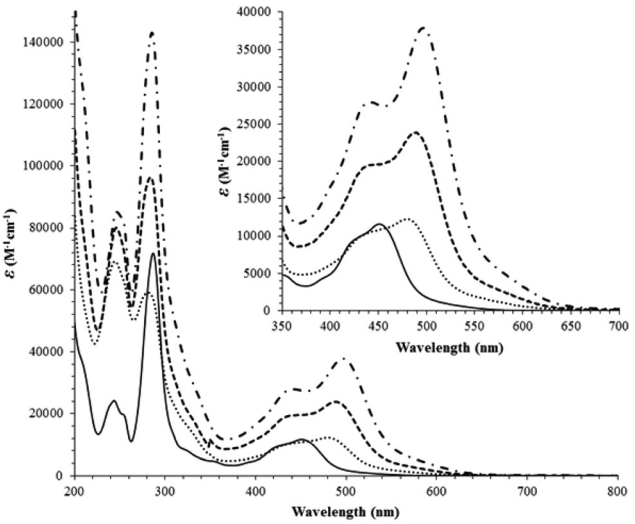

Fig. 8 Absorption spectra of complexes **RuL** (dot), **Ru_2L** (dash), **Ru_3L** (dash-dot) and **$[Ru(2,2'\text{-bpy})_3]^{2+}$** (solid line) recorded in acetonitrile solution at ambient temperature.

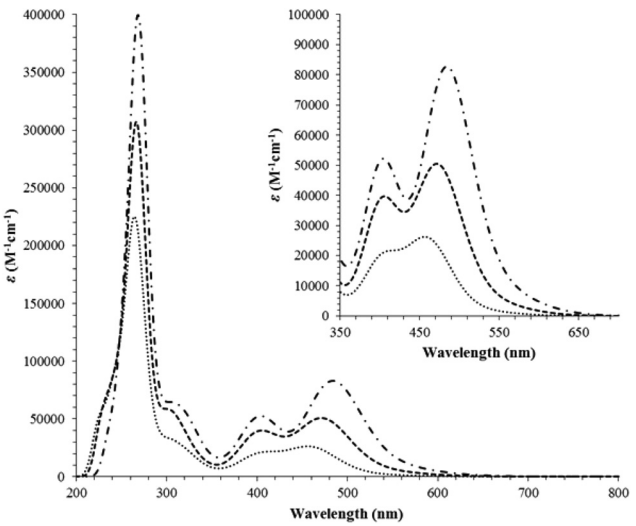

Fig. 9 TD-DFT simulated (PBE0/LANL2DZ; CPCM: CH_3CN) absorption spectrum for the complexes **RuL** (dot), **Ru_2L** (dash) and **Ru_3L** (dash-dot).

Table 3 Emission maxima, lifetime and quantum yield for the ligand, metal complexes and the reference

Compound	Luminescence, 298 K λ_{max}, nm	Lifetime τ, ns	Quantum yield Φ, %
L[a]	412	—	—
RuL^{2+} [b]	697	664	2.0
Ru_2L $^{4+}$ [b]	706	499	1.3
Ru_3L $^{6+}$ [b]	712	264	0.7
$[Ru(bpy)_3]^{2+}$ [b]	608	1100	9.5[c]

[a] In deaerated dichloromethane. [b] In deaerated acetonitrile. [c] From ref. 20.

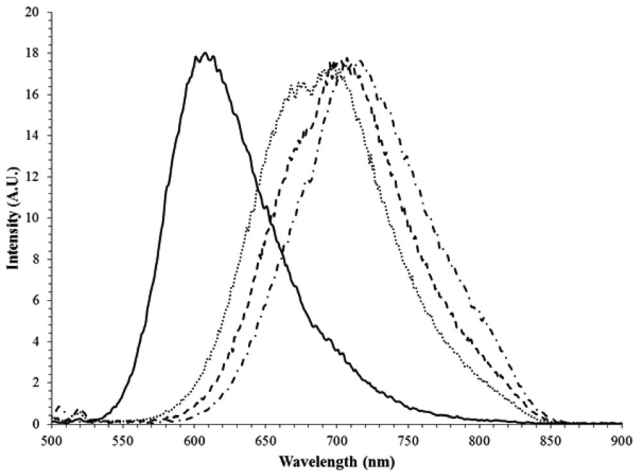

Fig. 10 Normalized emission spectra of complexes **RuL** (dot), **Ru_2L** (dash), **Ru_3L** (dash-dot) and **Ru(2,2′-bpy)$_3$** (solid line) recorded in acetonitrile solution at ambient temperature.

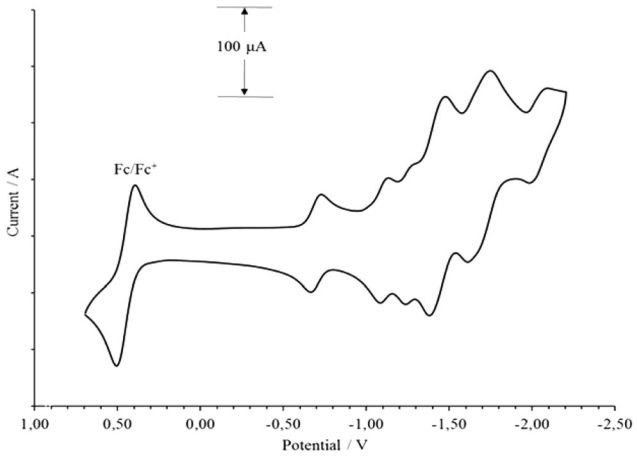

Fig. 11 Cyclic voltammogram of **Ru_3L** in degassed DMF solution showing ligand-based reduction waves with respect to Fc/Fc^+. Scan rate = 0.05 V s^{-1}.

four reduction processes. The first reversible and second quasi-reversible processes are located on the triazine moiety while the third and fourth quasi-reversible processes are related to the reduction of the 2,2′-bipyridyl units. Each complex undergoes a single reversible Ru^{2+}/Ru^{3+} metal-centered oxidation around 1.3 V. The presence of only one oxidation process in the case of **Ru_2L** and **Ru_3L** complexes is an indication of a lack of communication between the metal centers.

Previous reports of a triruthenium complex based on the 6,6′-di(pyridin-2″-yl)-4,4′-bipyrimidine ligand displayed enhanced communication between the metal centers, where three one-electron oxidations process were reported.[23] It is important to mention that in that instance, the metal–metal distance between the closest ruthenium ions is of 6.1 Å and of 11.0 Å between the peripheral Ru(II) metal ions (see Fig. S14†). As was mentioned previously, the metal-to-metal distances range between 12.8–13.6 Å in the case of the **Ru_3L** complex, which is significantly longer and might explain the absence of communication between the metals center. The DFT calculations (Fig. 12) were consistent with a primarily metal-based highest occupied molecular orbital (HOMO) (**RuL**: 76% Ru(II), 15% 2,2′-bpy, 9% **L**; **Ru_2L**: 76% Ru(II), 15% 2,2′-bpy, 10% **L**; **Ru_3L**: 76% Ru(II), 15% 2,2′-bpy, 8% **L**).

All of the complexes exhibit a minimum of five reversible one-electron ligand-based reduction processes). Introduction of several metal ions shifts the first reduction of the ligands to less negative potential in the order **Ru_3L** > **Ru_2L** > **RuL**. As shown in Fig. 12, the DFT calculations suggest that the lowest unoccupied molecular orbital (LUMO) and LUMO+1 of complexes **RuL** and **Ru_2L** have predominant contribution from the central 1,3,5-triazine ligand while LUMO+2 to LUMO+5 display contribution from the peripheral 2,2′-bipyridyl units (see Fig. S19–S21, ESI†). The first and second reduction processes were attributed to the reduction of the central ligand, more specifically, an extended orbital that includes the triazine core while the three subsequent reductions occurring at more negative potential were linked to reduction centered on the 2,2′-bipyridyl units, since their reduction potential are closely similar to the reported reduction values in the parent reference complex $[Ru(2,2'\text{-bpy})_3]^{2+}$. The case of complex **$Ru_3L$** is quite similar, the difference being that LUMO+2 shows predominant contributions from the central ligand instead of showing contribution from the peripheral 2,2′-bipyridyl units.

Table 4 Electrochemical data for the ligand, the $[(Ru(bpy)_2)_n(L)][(PF_6)_{2n}]$ family and related compounds[a]

Compound	Oxidation potential (V) (ΔE_p (mV))	Reduction potential (V) (ΔE_p (mV))					
L[b]	—	−1.16 (68)	−1.82[e]	−2.05[e]	−2.25[e]	—	—
2,2′-bpy[c]	—	—	—	−2.05[f]	—	—	—
RuL^{2+} [b]	1.31 (88)	−0.85 (59)	−1.35 (60)	−1.50 (63)	−1.76 (62)	−2.10 (87)	—
Ru_2L $^{4+}$ [b]	1.33 (112)	−0.76 (64)	−1.15 (56)	−1.40 (91)	−1.59 (52)	−1.69 (51)	−1.88 (65)
Ru_3L $^{6+}$ [b]	1.29 (88)	−0.70 (62)	−1.11 (48)	−1.26 (39)	−1.43 (99)	−1.70 (95)	−2.05 (89)
$Ru(2,2'\text{-bpy})_3^{2+}$	1.30[g]	—	—	−1.25[d]	−1.43[d]	−1.68[d]	—

[a] Potentials are in volts *vs.* SCE. Cyclic voltammetry was performed in DMF/*t*-$Bu_4N(PF_6)$ (0.1 M), recorded at 25 ± 1 °C with a sweep rate of 50 mV s^{-1}. All potentials are corrected *vs.* Fc/Fc^+. [b] In deaerated DMF. [c] From ref. 24. [d] From ref. 25. [e] Quasi-reversible process. [f] Irreversible process. [g] From ref. 26.

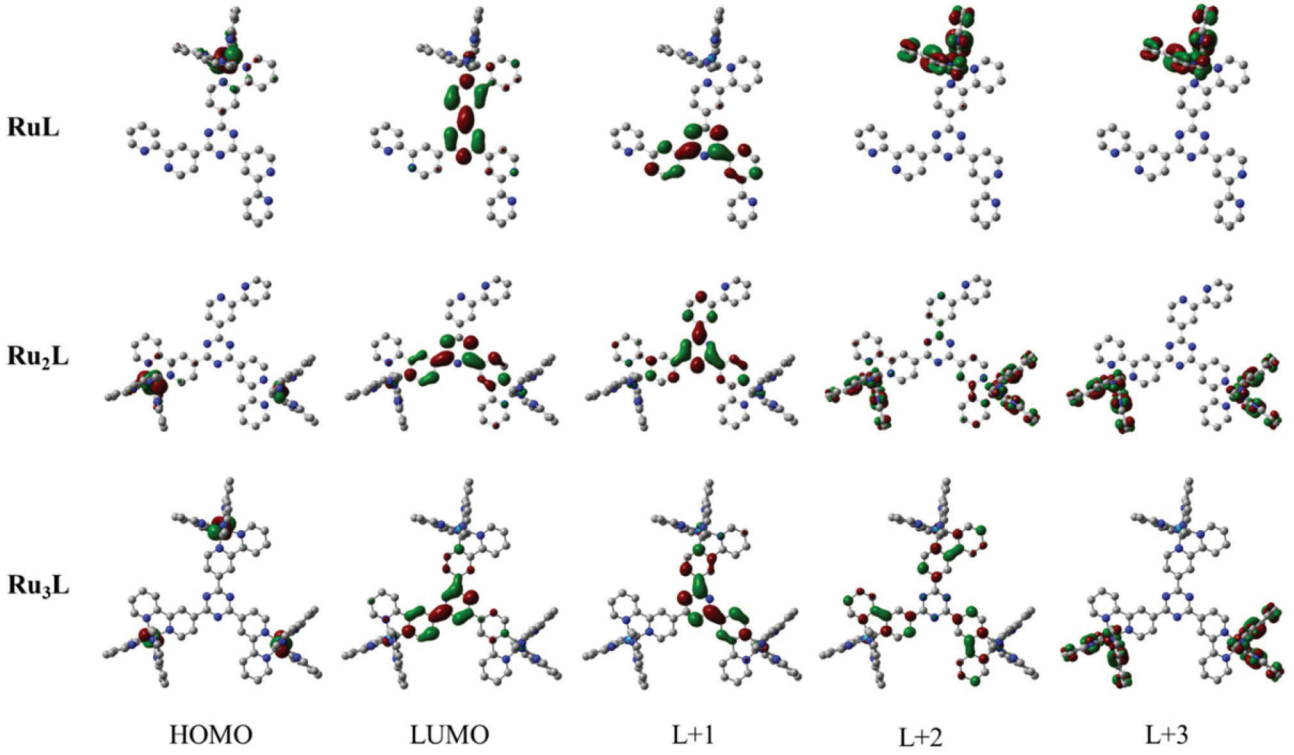

Fig. 12 Calculated Kohn–Sham frontier MOs of the metal complexes from DFT in (S = 0) ground state (PBE0/LANL2DZ; CPCM: CH_3CN).

More detailed calculations were performed on the reduced species to confirm this assignment (at the same level of theory previously described using an unrestricted formalism in the case of open shell systems). For the first reduction, the geometry of the metal complexes was optimized in the doublet state (S = 1/2) while both singlet (S = 0) and triplet (S = 1) geometries were calculated for the second reduction whereas doublet (S = 1/2) and quartet (S = 3/2) geometries were considered in the case of the third reduction. Only the geometries with the lowest energy are reported herein. Fig. 13 displays the electron-spin density plot for each reduced species and the corresponding values are shown in Tables S3–S5, S8–S10 and S13–S15 (ESI†). The results are in good agreement with the unpaired electrons being concentrated on the main triazine core of **L** for the first two reductions of the three metal complexes. In the case of the third reduction, the unpaired electrons in **RuL** are concentrated on both the triazine moiety and the peripheral 2,2′-bipyridine while it is concentrated mainly on the peripheral ligand in the case of **Ru_2L**. Finally, the unpaired electrons in **Ru_3L** are concentrated only over ligand **L**.

Conclusions

A family of $[(Ru(2,2'\text{-bpy})_2)_n(L)][(PF_6)_{2n}]$ complexes with n = 1–3 and L = tris-2″,4″,6″-(2,2′-bipyridin-4-yl)-1″,3″,5″-triazine have been prepared and characterized, and the X-ray crystal structures of both the ligand and $[(Ru(2,2'\text{-bpy})_2)_3(L)][(PF_6)_6]$ were determined. The ligand induced a bathochromic shift of the MLCT band in the absorption spectrum as compared to the parent complex $[Ru(2,2'\text{-bpy})_3][(PF_6)_2]$. More specifically, **$Ru_3$L** exhibits high intensity absorptions tailing out passed 600 nm. The central triazine component has a significant effect on the unoccupied molecule orbitals in spite of the fact that it is not directly bonded to the metal ions. This effect is most significant in the equilibrated ^{3}MLCT state which emits at a considerably lower energy than the archetypical $[Ru(2,2'\text{-bpy})_3]^{2+}$ complex. The use of **L** in the synthesis of multi-metallic dendrimers is underway and may prove to be a more versatile method of preparing such complexes as compared to creating new binding sites in metal complexes.[27]

Experimental

Materials and instrumentations

$RuCl_3 \cdot xH_2O$ was purchased from Pressure Chemical Corporation. Silver nitrate, potassium hexafluorophosphate, 2,2′-bipyridine, sodium hydride and hydrazine hydrate were purchased from Aldrich. All were used without further purification. ACS grade solvents were purchased from VWR and Fisher. Nuclear magnetic resonance (NMR) spectra were recorded in $CDCl_3$ and CD_3CN at 25 °C on a Bruker AV-400 spectrometer at 400 MHz for ^{1}H NMR and at 100 MHz for ^{13}C NMR. Chemical shifts (δ) are reported in parts per million

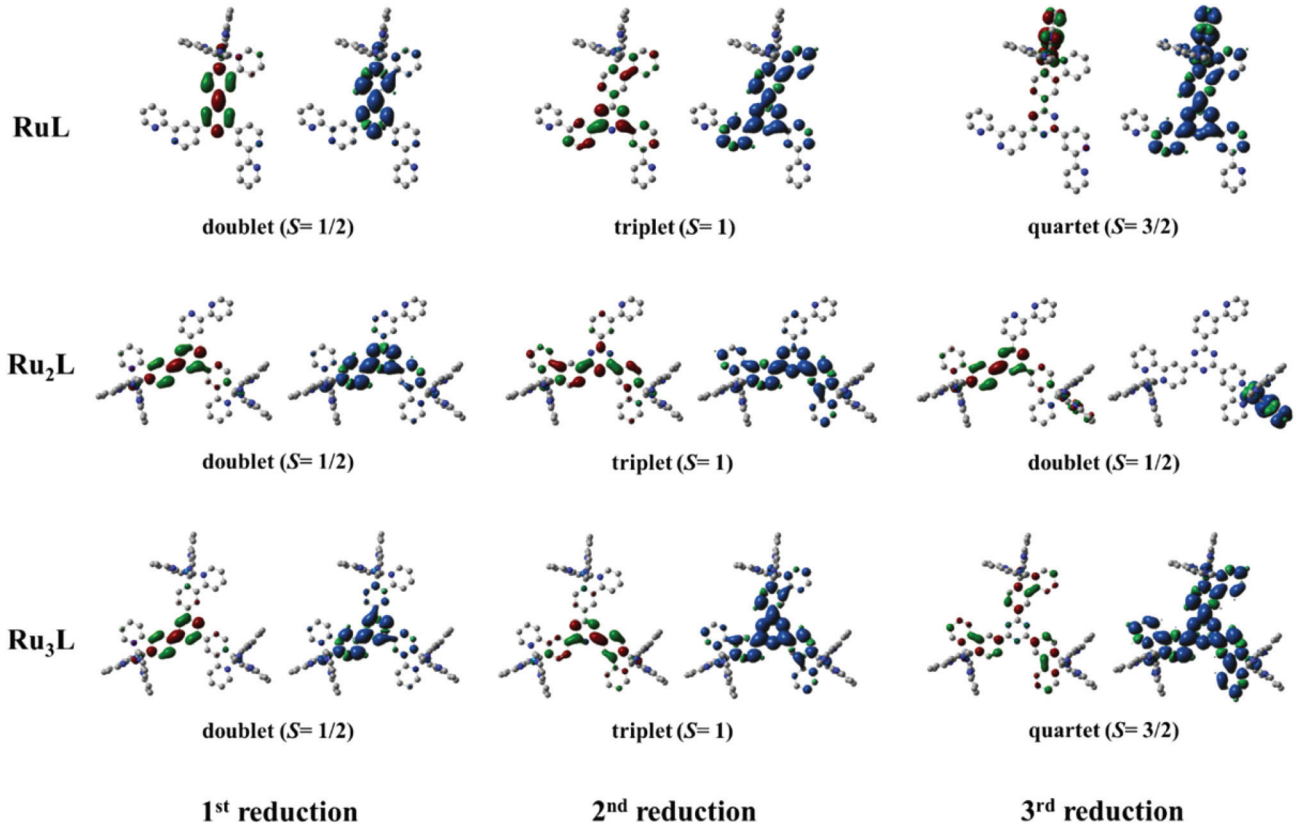

Fig. 13 Kohn-Sham molecular orbitals (left) of the DFT-optimized structure (uPBE0/LANL2DZ; CPCM: CH_3CN) for the first, second and third reduced states of the Ru(II) complexes and their electron-spin density plots (right).

(ppm) relative to TMS, and are referenced to the residual solvent signal (δ = 1.94 ppm for acetonitrile-d_3 and 7.26 ppm for chloroform-d_1). Absorption and emission spectra were measured in deaerated spectrograde solvent at room temperature on a Cary 500i UV-Vis-NIR Spectrophotometer and a Cary Eclipse Fluorescence Spectrophotometer, respectively. For the luminescence lifetimes, an Edinburgh OB 900 single-photon-counting spectrometer was used, employing a Hamamatsu PLP2 laser diode as pulse (wavelength output, 408 nm; pulse width, 59 ps).

Emission quantum yields were measured at room temperature using the optically dilute method.[28] $[Ru(bpy)_3][(PF_6)_2]$ in deaerated acetonitrile solution was used as quantum yield standard, assuming a value of 0.095.[20] Electrochemical measurements were carried out in argon-purged dimethylformamide at room temperature with a BAS CV50W multipurpose potentiostat. The working electrode was a glassy carbon electrode. The counter electrode was a Pt wire, and the pseudo-reference electrode was a silver wire. The reference was set using an internal 1 mM ferrocene/ferrocenium sample at 450 mV *vs.* SCE in dimethylformamide. The concentration of the compounds was of about 1 mM. Tetrabutylammonium hexafluorophosphate (TBAP) was used as the supporting electrolyte and its concentration was 0.10 M. Cyclic voltammograms were obtained at scan rates of 25, 50, 100, 200, and 500 mV s^{-1}. For reversible processes, half-wave potentials (*vs.* SCE) were measured with differential pulse voltammetry (DPV) experiments performed with a step rate of 4 mV, a pulse height of 25 mV, and a frequency of 15 Hz. For irreversible reduction processes, the cathodic peak was used as *E*. The criteria for reversibility were the close to unity ratio of the intensities of the cathodic and anodic currents, and the constancy of the peak potential on changing scan rate. Experimental uncertainties are as follows: absorption maxima, ±2 nm; molar absorption coefficient, 10%; emission maxima, ±5 nm; excited state lifetimes, 10%; luminescence quantum yields, 20%; redox potentials, ±10 mV. The microanalyses and the mass spectrometry analyses were performed at the Elemental Analysis Service and the Regional Mass Spectrometry Centre of the Université de Montréal.

X-ray structure determination

X-Ray diffraction data collection for the ligand was carried out on a Bruker APEX II DUO Kappa-CCD diffractometer equipped with an Oxford Cryosystem liquid N_2 device, using Cu-Kα radiation (λ = 1.54178 Å). The crystal–detector distance was 38 mm. The cell parameters were determined (APEX2 software) 39 from reflections taken from three sets of 12 frames, each at 10 s exposure. The structure was solved by direct methods using the program SHELXS-97. The refinement and all further

calculations were carried out using SHELXL-97. The H-atoms were included in calculated positions and treated as riding atoms using SHELXL default parameters. The non-H atoms were refined anisotropically, using weighted full-matrix least-squares on F^2. A semi-empirical absorption correction was applied using SADABS in APEX2; transmission factors: T_{min}/T_{max} = 0.8683/0.9309.

The metal complex data collection was carried out on a Bruker Venture Metaljet diffractometer equipped with an Oxford Cryosystem liquid N_2 device, using Ga-Kα radiation (λ = 1.34139 Å). The cell parameters were determined (APEX2 software) from reflections taken from three sets of 100 frames. The structure was solved by direct methods using the program Olex2.[29] The refinement and all further calculations were carried out using Olex2. The H-atoms were included in calculated positions and treated as riding atoms using OLEX2 default parameters. The non-H atoms were refined anisotropically, using weighted full-matrix least-squares on F^2. A semi-empirical absorption correction was applied using SADABS in APEX2; transmission factors: T_{min}/T_{max} = 0.6004/0.7511. More details are provided in the ESI.† CCDC 964307 and CCDC 1017168 contain the supplementary crystallographic data for this paper.

Computational details

Gaussian 09, Revision D.01 was used for all theoretical calculations discussed herein.[30] The molecular structure of the three metal complexes was fully optimized with CPCM acetonitrile solvation model in absence of constraints at Density Functional Theory (DFT) level. In particular, the hybrid PBE0 functional,[31] casting 25% of HF exchange in the PBE functional was applied.[32] A double zeta valence basis set was used for all atoms but the Ru ones which were described by the Los Alamos pseudo potential and corresponding basis set.[33]

Details of optimized structures are given in Tables S1, S2, S6, S7, S11 and S12, ESI.† No imaginary frequencies were obtained when frequency calculations on optimized geometries were performed. The molecular structure of the reduced metal complexes was fully optimized at the same level of theory but using an unrestricted formalism in the case of open shell systems. The values of $<S^2>$ were monitored and did not show major spin contamination. GaussView 5.0.8 and Chemissian 2.200 software were used for data analysis, visualization and surface plots.[34]

Synthesis of the ligand and metal complexes

Compounds $Ru(bpy)_2Cl_2$ starting material was synthesized as previously described.[35] Solvents were removed under reduced pressure using a rotary evaporator unless otherwise stated.

Synthesis of tris-2″,4″,6″-(2,2′-bipyridin-4-yl)-1″,3″,5″-triazine (L). A oven-dried 10 mL microwave vial was charged with 4-cyano-2,2′-bipyridine (100 mg, 0.55 mmol) and sodium hydride (2 mg, 0.08 mmol). The vial was equipped with a stirrer and sealed. An alternance of vacuum and N_2 was apply at least three times and the mixture was left at 190 °C for 8 h. The resulting brown solid was cooled to room temperature before adding ethanol (10 mL). The slurry was sonicated for 5 minutes and solvent was evaporated under vacuum. Water (10 mL) was added and the resulting mixture was filtered over paper. The resulting precipitate was washed with ethanol (10 mL), yielding a pure colorless solid (40 mg, 40%) which was used without further purification. ^{1}H NMR ($CDCl_3$, 400 MHz, 330 K): δ (ppm) 9.74 (s, 3H, Ha,a′,a″), 9.03 (d, J_d = 5.0 Hz, 3H, Hb,b′,b″), 8.88 (d, J_d = 4.2 Hz, 3H, Hd,d′,d″), 8.76 (d, J_d = 4.9 Hz, 3H, Hc,c′,c″), 8.59 (d, J_d = 7.9 Hz, 3H, Hg,g′,g″), 7.97 (t, J_t = 7.8 Hz, 3H, Hf,f′,f″), 7.47 (t, J_t = 5.3 Hz, 3H, He,e′,e″). ^{13}C{1H}NMR ($CDCl_3$-d_1, 400 MHz, 330 K): 171.5, 157.5, 155.5, 150.3, 149.4, 143.6, 137.0, 124.1, 122.5, 121.4, 120.0. ESI-MS (TFA : CH_2Cl_2): $[M]^+$ = 544.4.

Synthesis of [(Ru(2,2′-bpy)$_2$)L][(PF$_6$)$_2$] (RuL). A 100 mL round-bottomed flask was charged with ligand **L** (50 mg, 0.092 mmol) and dichloromethane (25 mL). $Ru(bpy)_2Cl_2$ (45 mg, 0.092 mmol) and silver nitrate (40 mg, 0.23 mmol) were separately dissolved in methanol (25 mL each). The methanol solutions were then added dropwise to the flask over 30 minutes with vigorous stirring. The reaction mixture was left at reflux for 24 h. After this time, a few drops of hydrazine were added to convert any Ru(III) to Ru(II). The resulting slurry was filtered over a fine glass frit. The filtrate was extracted with dichloromethane and evaporated under vacuum. The residue was then purified on silica column using 7 : 2 : 1 (MeCN : H_2O : KNO_3 sat.). The counter-anions were exchanged twice with a solution of KPF_6 in water (10 eq.), resulting in the precipitation a pure red solid (33 mg, 29%).

^{1}H NMR (CD_3CN, 400 MHz, 330 K): δ (ppm) 9.62 (s, 1H), 9.02 (s, 1H), 8.65–8.57 (m, 6H), 8.46 (d, J_d = 8.0 Hz, 1H), 8.41 (d, J_d = 4.8 Hz, 2H), 8.28 (d, J_d = 3.9 Hz, 2H), 8.16–8.08 (m, 5H), 8.02–7.96 (m, 4H), 7.81–7.69 (m, 7H), 7.50–7.36 (m, 5H), 7.34 (t, J_t = 5.1 Hz, 2H). ^{13}C{1H}NMR (MeCN-d3, 400 MHz, 330 K): 157.8, 157.7, 157.6, 155.6, 152.9, 152.6, 152.4, 151.1, 150.3, 139.2, 139.1, 138.2, 128.8, 128.7, 128.6, 125.7, 125.5, 125.4, 123.1, 121.8, 119.8. ESI-MS (TFA : MeCN): $[M]^{2+}$ = 478.61752 (theoretical = 478.61637); $[M + (PF_6)]^+$ = 1102.19843 (theoretical = 1102.19747). Calc. for $C_{53}H_{37}N_{13}RuP_2F_{12}\cdot 3CH_2Cl_2$: C, 44.79; H, 2.89; N, 12.12. Found: C, 44.72; H, 3.09; N, 12.15%.

Synthesis of [(Ru(2,2′-bpy)$_2$)$_2$L][(PF$_6$)$_4$] (Ru$_2$L). A 100 mL round-bottomed flask was charged with **L** (50 mg, 0.092 mmol) and dichloromethane (25 mL). $Ru(bpy)_2Cl_2$ (90 mg, 0.18 mmol) and silver nitrate (80 mg, 0.46 mmol) were separately dissolved in methanol (25 mL each). The methanol solutions were then added dropwise to the flask over 30 minutes with vigorous stirring. The reaction mixture was left under reflux for 24 h. After this time, a few drops of hydrazine were added to convert any Ru(III) to Ru(II). The resulting slurry was filtered over a glass frit. The filtrate was extracted with dichloromethane and evaporated under vacuum. The residue was then purified on silica column using 7 : 2 : 1 (MeCN : H_2O : KNO_3 sat.). The counter-anions were exchanged twice with a solution of KPF_6 in water (10 eq.), resulting in the precipitation of a pure red solid (18 mg, 20%).

^{1}H NMR (CD_3CN, 400 MHz, 330 K): δ (ppm) 9.63 (s, 2H), 9.57 (s, 1H), 9.06 (d, J_d = 4.4 Hz, 1H), 8.93 (d, J_d = 8.1

Hz, 2H), 8.82–8.78 (m, 2H), 8.68 (d, J_d = 5.6 Hz, 2H), 8.54 (d, J_d = 7.0 Hz, 8H), 8.19–8.06 (m, 13H), 7.87 (d, J_d = 5.1 Hz, 2H), 7.82–7.76 (m, 8H), 7.62 (t, J_t = 6.3 Hz, 1H), 7.51–7.40 (m, 10H). ^{13}C{1H}NMR (MeCN-d_3, 400 MHz, 330 K): 171.0, 157.9, 157.8, 157.6, 157.4, 154.0, 152.7, 152.5, 144.1, 139.0, 138.9, 129.0, 128.6, 128.5, 126.6, 126.0, 125.3, 123.2. ESI-MS (TFA : MeCN): $[M]^{4+}$ = 342.81915 (theoretical = 342.81837), $[M + (PF_6)]^{3+}$ = 505.41342 (theoretical = 505.41274); $[M + 2(PF_6)]^{2+}$ = 830.60011 (theoretical = 830.60147). Calc. for $C_{73}H_{53}N_{17}Ru_2P_4F_{24}\cdot H_2O$: C, 44.55; H, 2.82; N, 12.10. Found: C, 44.27; H, 3.17; N, 11.67%.

Synthesis of $[(Ru(2,2'\text{-bpy})_2)_3L][(PF_6)_6]$ (Ru_3L). A 25 mL round-bottomed flask was charged with **L** (25 mg, 0.046 mmol), $Ru(bpy)_2Cl_2$ (66.84 mg, 0.138 mmol) and silver nitrate (68 mg, 0.40 mmol). A mixture of ethylene glycol : water (9 : 1) (20 mL) was added and then left at reflux for 4 h. The resulting solution was added to an aqueous KPF_6 solution. The resulting red precipitate was filtered over celite and dissolved in a minimum amount of acetonitrile. The solution was reduced under vacuum and the residue was purified by two silica chromatography columns, using 7 : 2 : 1 ($MeCN : H_2O : KNO_3$ sat.) for the first one, and a gradient of 7 : 3 (MeCN : HCl 0.5 M) to 7 : 2 : 1 ($MeCN : H_2O : KNO_3$ sat.) for the second one. A solution of 10 eq. KPF_6 was then added, resulting in the precipitation of the title compound as a pure red solid (77 mg, 61%).

Alternatively, a 20 mL microwave vial from Biotage® was loaded with ligand L ((25 mg, 0.046 mmol), $Ru(bpy)_2Cl_2$ (66.84 mg, 0.138 mmol) and silver nitrate (68 mg, 0.40 mmol). A mixture of ethylene glycol : water (9 : 1) (20 mL) was added and the vial was left under microwave irradiation (400 W) for 15 minutes. As in the thermal reaction, the resulting solution was poured into an aqueous KPF_6 solution followed by the same purification procedure with a similar yield. The same procedure has been used in the synthesis of $[(Ru(2,2'\text{-bpy})_2)_3L][(BF_4)_6]$, except that the metathesis was done using the $NaBF_4$ salt instead of KPF_6 to induce the precipitation of the desired product. No significant shift in proton resonances by ^{1}H NMR were observed with the BF_4 species.

^{1}H NMR (CD_3CN, 400 MHz, 330 K): δ (ppm) 9.62 (s, 3H), 8.93 (d, J_d = 8.1 Hz, 3H), 8.70 (d, J_d = 6.1 Hz, 3H), 8.55–8.52 (m, 12H), 8.16–8.04 (m, 18H), 7.83 (d, J_d = 5.6 Hz, 3H), 7.80–7.74 (m, 12H), 7.49–7.37 (m, 15H). ^{13}C{1H}NMR (MeCN-d_3, 400 MHz, 330 K): 171.3, 159.7, 157.9, 157.8, 157.7, 157.6, 157.5, 154.0, 152.7, 152.6, 152.5, 143.9, 139.0, 128.9, 128.6, 125.3, 123.5. ESI-MS (TFA : MeCN): $[M + (PF_6)]^{5+}$ = 386.25499 (theoretical = 386.25638), $[M + 2(PF_6)]^{4+}$ = 519.06197 (theoretical = 519.06166), $[M + 3(PF_6)]^{3+}$ = 740.07207 (theoretical = 740.06947); $[M + 4(PF_6)]^{2+}$ = 1182.09508 (theoretical = 1182.09293). Anal. Calc. for $C_{93}H_{69}N_{21}Ru_3P_6F_{36}\cdot H_2O$: C, 41.81; H, 2.68; N, 11.01. Found: C, 42.09; H, 2.62; N, 11.08%.

Acknowledgements

GSH thanks the Natural Sciences and Engineering Research Council (NSERC) of Canada and the Université de Montréal's Direction des Relations Internationales for financial aid. BLM thanks Dr. Thierry Maris and Dr Michel Simard for their assistance with the X-ray diffraction experiment and useful crystallographic discussions. We are grateful to Compute Canada and to UdeM NMR, EA, XRD and MS services for their help.

Notes and references

1 P. Gamez and J. Reedijk, *Eur. J. Chem.*, 2006, **1**, 29.
2 (*a*) P. Gamez, P. de Hoog, M. Lutz, A. L. Spek and J. Reedijk, *Inorg. Chim. Acta*, 2003, **351**, 319; (*b*) J. Roeser, K. Kailasam and A. Thomas, *ChemSusChem*, 2012, **5**, 1793; (*c*) M. Shafiee, A. R. Khosropour, I. Mohammmadpoor-Baltork, M. Moghadam, S. Tangestaninejad and V. Mirkhani, *Catal. Sci. Technol.*, 2012, **2**, 2440.
3 (*a*) G. d'Atri, P. Gomarasca, G. Resnati, G. Tronconi, C. Scolastico and C. R. Sirtori, *J. Med. Chem.*, 1984, **27**, 1621; (*b*) R. Menicagli, S. Samaritani, G. Signore, F. Vaglini and L. Dalla Via, *J. Med. Chem.*, 2004, **47**, 4649; (*c*) Q. Wang, G. Liu, R. Shao and R. Huang, *Heteroat. Chem.*, 2003, **14**, 542.
4 (*a*) D. R. Anderson and J. M. Holovka, *J. Polym. Sci., Part A: Polym. Chem.*, 1966, **4**, 1689; (*b*) A. Modak, J. Mondal, M. Sasidharan and A. Bhaumik, *Green Chem.*, 2011, **13**, 1317; (*c*) S. Ren, R. Dawson, A. Laybourn, J.-X. Jiang, Y. Khimyak, D. J. Adams and A. I. Cooper, *Polym Chem.*, 2012, **3**, 928.
5 K. Koizumi, N. Kuboyama, K. Tomono, A. Tanaka, A. Ohki, H. Kohno, K. Wakabayashi and P. Böger, *Pestic. Sci.*, 1999, **55**, 633.
6 (*a*) M. Fujita, D. Oguro, M. Miyazawa, H. Oka, K. Yamaguchi and K. Ogura, *Nature*, 1995, **378**, 469; (*b*) T. Kusukawa and M. Fujita, *J. Am. Chem. Soc.*, 2002, **124**, 13576; (*c*) B. F. Abrahams, S. R. Batten, H. Hamit, B. F. Hoskins and R. Robson, *Angew. Chem., Int. Ed.*, 1996, **35**, 1690; (*d*) D. Tian, Q. Chen, Y. Li, Y.-H. Zhang, Z. Chang and X.-H. Bu, *Angew. Chem., Int. Ed.*, 2014, **53**, 837; (*e*) Q. Tang, S. Liu, Y. Liu, D. He, J. Miao, X. Wang, Y. Ji and Z. Zheng, *Inorg. Chem.*, 2014, **53**, 289; (*f*) D. F. S. Gallis, L. E. S. Rohwer, M. A. Rodriguez and T. M. Nenoff, *Chem. Mater.*, 2014, **26**, 2943.
7 (*a*) A. K. Pal and G. S. Hanan, *Chem. Soc. Rev.*, 2014, **43**, 6184; (*b*) A. K. Pal, S. Serroni, N. Zaccheroni, S. Campagna and G. S. Hanan, *Chem. Sci.*, 2014, **5**, 4800; (*c*) A. K. Pal, N. Zaccheroni, S. Campagna and G. S. Hanan, *Chem. Commun.*, 2014, **50**, 6846; (*d*) M.-P. Santoni, G. S. Hanan, A. Proust, B. Hasenknopf, F. Nastasi and S. Campagna, *Chem. Commun.*, 2011, **47**, 3586; (*e*) M.-P. Santoni, S. Campagna, F. Nastasi, G. S. Hanan, I. Ciofini and B. Hasenknopf, *Dalton Trans.*, 2013, **42**, 5281.
8 (*a*) O. Johansson, L. O. Johannissen and R. Lomoth, *Chem. – Eur. J.*, 2009, **15**, 1195; (*b*) L.-F. Tan, J. Liu, J. L. Shen, X.-H. Liu, L.-L. Zeng and L.-H. Jin, *Inorg. Chem.*, 2012, **51**, 4417.

9 P. R. Ashton, R. Ballardini, V. Balzani, E. C. Constable, A. Credi, O. Kocian, S. J. Langford, J. A. Preece, L. Prodi, E. R. Schofield, N. Spencer, J. F. Stoddart and S. Wenger, *Chem. – Eur. J.*, 1998, **4**, 2413.
10 (*a*) A. Reynald and E. Palomares, *Eur. J. Inorg. Chem.*, 2011, **29**, 4509; (*b*) F. Matar, T. H. Ghaddar, K. Walley, T. DosSantos, J. R. Durrant and B. O'Regan, *J. Mater. Chem.*, 2008, **18**, 4246.
11 (*a*) S. Campagna, S. Serroni, F. Punteriero, F. Loiseau, L. De Cola, C. J. Kleverlaan, J. Becher, A. P. Sørensen, P. Hascoat and N. Thorup, *Chem. Eur. J. Chem.*, 2002, **8**, 4461; (*b*) J. Otsuki, A. Imai, K. Sato, D.-M. Li, M. Hosoda, M. Owa, T. Akasaka, I. Yoshikawa, K. Araki, T. Suenobu and S. Fukuzumi, *Chem. – Eur. J.*, 2008, **14**, 2709.
12 A. Bessette and G. S. Hanan, *Chem. Soc. Rev.*, 2014, **43**, 3342.
13 Y. Kobuke, *Struct. Bonding*, 2006, **121**, 49.
14 Y.-Q. Fang and G. S. Hanan, *Synlett*, 2003, 852.
15 F. H. Case, *J. Org. Chem.*, 1966, **31**, 2398.
16 E. E. Pérez-Cordero, C. Campana and L. Echegoyen, *Angew. Chem., Int. Ed.*, 1997, **36**, 137.
17 (*a*) A. Mitra, P. J. Seaton, R. A. Assarpour and T. Williamson, *Tetrahedron*, 1998, **54**, 15489; (*b*) C. Lavigueur, E. J. Foster and V. E. Williams, *J. Am. Chem. Soc.*, 2008, **130**, 11791.
18 E. Castellucci, L. Angeloni, G. Marconi, E. Venuti and I. Baraldi, *J. Phys. Chem.*, 1990, **94**, 1740.
19 E. Ronca, F. De Angelis and S. Fantacci, *J. Phys. Chem. C*, 2014, **118**, 17067.
20 A. K. Suzuki, A. Kobayashi, S. Kaneko, K. Takehira, T. Yoshihara, H. Ishida, Y. Shiina, S. Oishica and S. Tobita, *Phys. Chem. Chem. Phys.*, 2009, **11**, 9850.
21 J. V. Caspar, E. M. Kober, B. P. Sullivan and T. J. Meyer, *J. Am. Chem. Soc.*, 1982, **104**, 630.
22 (*a*) E. A. Medlycott, G. S. Hanan, F. Loiseau and S. Campagna, *Chem. – Eur. J.*, 2007, **13**, 2837–2846; (*b*) M. I. J. Polson, E. A. Medlycott, G. S. Hanan, L. Mikelsons, N. J. Taylor, M. Watanabe, Y. Tanaka, F. Loiseau, R. Passalacqua and S. Campagna, *Chem. – Eur. J.*, 2004, **10**, 3640; (*c*) E. A. Medlycott, K. A. Udachin and G. S. Hanan, *Dalton Trans.*, 2007, 430; (*d*) E. Ioachim, E. A. Medlycott, G. S. Hanan, F. Loiseau, V. Ricevuto and S. Campagna, *Inorg. Chem. Commun.*, 2005, **8**, 559.
23 M. I. J. Polson, G. S. Hanan, N. J. Taylor, B. Hasenknopf and R. Thouvenot, *Chem. Commun.*, 2004, 1314.
24 P. R. Murray, S. Crawford, A. Dawson, A. Delf, C. Findlay, L. Jack, E. J. L. McInnes, S. Al-Musharafi, G. S. Nichol, I. Oswald and L. J. Yellowlees, *Dalton Trans.*, 2012, **41**, 201.
25 T. Matsumura-Inoue, *J. Electroanal. Chem.*, 1979, **95**, 109.
26 S. Saji and T. Aoyagui, *J. Electroanal. Chem. Interfacial Electrochem.*, 1975, **58**, 40.
27 (*a*) K. O. Johansson, J. A. Lotoski, C. C. Tong and G. S. Hanan, *Chem. Commun.*, 2000, 819; (*b*) F. Loiseau, R. Passalacqua, S. Campagna, M. I. J. Polson, Y.-Q. Fang and G. S. Hanan, *Photochem. Photobiol. Sci.*, 2002, 982; (*c*) Y.-Q. Fang, M. I. J. Polson and G. S. Hanan, *Inorg. Chem.*, 2002, **42**, 5.
28 (*a*) A. T. R. Williams, S. A. Winfield and J. N. Miller, *Analyst*, 1983, **108**, 1067; (*b*) A. M. Brouwer, *Pure Appl. Chem.*, 2011, **83**, 2213; (*c*) C. Würth, M. Grabolle, J. Pauli, M. Spieles and U. Resch-Genger, *Nat. Protoc.*, 2013, **8**, 1535.
29 O. V. Dolomanov, L. J. Bourhis, R. J. Gildea, J. A. K. Howard and H. Puschmann, *J. Appl. Crystallogr.*, 2009, **42**, 339.
30 M. J. Frisch, G. W. Trucks, H. B. Schlegel, G. E. Scuseria, M. A. Robb, J. R. Cheeseman, G. Scalmani, V. Barone, B. Mennucci, G. A. Petersson, H. Nakatsuji, M. Caricato, X. Li, H. P. Hratchian, A. F. Izmaylov, J. Bloino, G. Zheng, J. L. Sonnenberg, M. Hada, M. Ehara, K. Toyota, R. Fukuda, J. Hasegawa, M. Ishida, T. Nakajima, Y. Honda, O. Kitao, H. Nakai, T. Vreven, J. A. Montgomery Jr., J. E. Peralta, F. Ogliaro, M. Bearpark, J. J. Heyd, E. Brothers, K. N. Kudin, V. N. Staroverov, R. Kobayashi, J. Normand, K. Raghavachari, A. Rendell, J. C. Burant, S. S. Iyengar, J. Tomasi, M. Cossi, N. Rega, J. M. Millam, M. Klene, J. E. Knox, J. B. Cross, V. Bakken, C. Adamo, J. Jaramillo, R. Gomperts, R. E. Stratmann, O. Yazyev, A. J. Austin, R. Cammi, C. Pomelli, J. W. Ochterski, R. L. Martin, K. Morokuma, V. G. Zakrzewski, G. A. Voth, P. Salvador, J. J. Dannenberg, S. Dapprich, A. D. Daniels, Ö. Farkas, J. B. Foresman, J. V. Ortiz, J. Cioslowski and D. J. Fox, *Gaussian 09, Revision D.01*, Gaussian, Inc., Wallingford, CT, 2009.
31 C. Adamo and V. Barone, *J. Chem. Phys.*, 1999, **110**, 6158.
32 (*a*) J. P. Perdew, K. Burke and M. Ernzerhof, *Phys. Rev. Lett.*, 1997, **78**, 1396; (*b*) J. P. Perdew, K. Burke and M. Ernzerhof, *Phys. Rev. Lett.*, 1996, **77**, 3865.
33 (*a*) T. H. Dunning Jr. and P. J. Hay, in *Modern Theoretical Chemistry*, ed. H. F. Schaefer III, Plenum, New York, 1976, vol. 3, p. 1; (*b*) P. J. Hay and W. R. Wadt, *J. Chem. Phys.*, 1985, **82**, 270; (*c*) P. J. Hay and W. R. Wadt, *J. Chem. Phys.*, 1985, **82**, 299; (*d*) T. H. Dunning Jr. and P. J. Hay, in *Methods of Electronic Structure Theory*, ed. H. F. Schaefer III, Plenum Press, New York, 1977, vol. 2; (*e*) W. R. Wadt and P. J. Hay, *J. Chem. Phys.*, 1985, **82**, 284.
34 L. Skripnikov, *Chemissian*, V2.200, 2005–2011.
35 B. P. Sullivan, D. J. Salmon and T. J. Meyer, *Inorg. Chem.*, 1978, **17**, 3334.